Three-dimensional finite-element simulations of the self-organized growth of quantum dot superlattices

P. Liu,[1] Y. W. Zhang,[2,3,*] and C. Lu[1]
[1]*Institute of High-Performance Computing, Singapore*
[2]*Department of Materials Science, National University of Singapore, Singapore*
[3]*Institute of Materials Research and Engineering, Singapore*
(Received 26 February 2003; revised manuscript received 27 June 2003; published 20 November 2003)

Controlling the self-organized growth of quantum dot superlattices to achieve perfect dot arrays has been studied through three-dimensional computer simulations. A growth window has been identified in which the self-organized quantum dots are arranged in a body-centered tetragonal superlattice with a fixed dot spacing irrespective of growth rates. However, the size of the quantum dots can be tuned through the change of growth rate. Surprisingly, the ordering of the self-organized quantum dot superlattices is controlled by the ordering of strain energy density maxima, which is in contrast with the previous understanding that the ordering of the self-organized quantum dot superlattice is controlled by the ordering of the strain energy density minima. This provides a guideline for the fabrication of quantum dot superlattices.

DOI: 10.1103/PhysRevB.68.195314 PACS number(s): 68.55.−a, 68.35.Fx, 68.65.Cd, 81.07.Ta

I. INTRODUCTION

Quantum dot superlattices are nanometer-sized semiconductor structures, which are one of the most rapidly developing areas of current semiconductor research. They present the utmost challenge to nanotechnology, making possible fascinating novel devices, such as LED's, detectors, data memory devices, lasers, and single electron transistors.[1,2] However, the fabrication of quantum dot superlattices with a uniform and regular array is still a challenging issue that defies practical applications. Due to the scientific interest and the wide potential applications, enormous effort has been given to tackle this challenge.[3]

The self-organization of quantum dots that spontaneously form during heteroepitaxial growth has recently been observed in many materials systems,[4–7] providing a potential way to quantum dot fabrication. However, the present understanding of the phenomenon of self-organization, which is essential to attaining this target, is still rudimentary. The stringent requirements of small size, defect-free shape, uniformity, and regularity make the growth of ordered quantum dot superlattices through self-organization still a daunting task.[8–20] The central issue is to control the self-organization.

The formation of quantum dots in heteroepitaxial film systems is due to the morphological instability driven by the strain energy reduction induced by the lattice mismatch between the film and the substrate.[21–25] During the formation of defect-free dots, the total strain energy is decreased while the total surface energy is increased. Since the total free energy is reduced, the surface roughening is energetically favorable at long wavelengths, leading to the self-organized formation of quantum dots.

The self-organization of quantum dots along the growth direction during the growth of quantum dot superlattices has shown a marked ordering with increasing number of growth layers. So far, no experimental method has succeeded in producing reproducibly identical ordered quantum dots in superlattices. It is believed that this ordering is due to the influence of the buried islands.[5,12–15,26,27] It is also believed that elastic anisotropy plays a role in the ordering.[5,14,15] Previous results under annealing conditions have shown that this ordering can also be achieved by controlling the spacer layer thickness and interruption time.[20] So far it is generally believed that this ordering is due to the ordering of the strain energy minimum on the spacer layer surface.[5,12–16,20] However, it will be shown that this is not the only underlying physical reason for the self-assembly.

In this paper, attention is focused on the self-assembly of quantum dot superlattices under growth. Massive parametric computations were carried out to identify the system parameters, which are crucial for controlling the self-organized growth of quantum dot superlattices. It is found that the growth rate, growth time, and spacer layer thickness are the most important parameters for growing ordered arrays of quantum dot superlattices. Most importantly, it is observed that there is a growth window in which a perfect body-centered tetragonal (bct) quantum dot superlattice with a fixed lattice spacing can be achieved irrespective of growth rate. It is noted that the anticorrelation for this ordering is not due to the elastic anisotropy effect,[5,15] but due to the adjustment of the spacer layer thickness, growth rate, and growth time.

More interestingly, with the variation of the growth rate within the window, the size of the quantum dots can be tuned while the spacing of the bct quantum dot superlattice remains unchanged. Surprisingly, we have identified a new underlying physics for the ordering of the self-organized quantum dot superlattices, that is, the ordering can be controlled by the ordering of the strain energy density maxima on the spacer layer surface, which is in contrast with the common understanding that the ordering of the quantum dots in a superlattice is controlled by the ordering of the strain energy density minima. In addition, some of the previous results revealed in annealing conditions[20] can also be extended to growth conditions. The ordered bct superlattice can also be obtained through annealing. The dot ordering is sensitive to the spacer layer thickness. When the spacer layer is thin, a

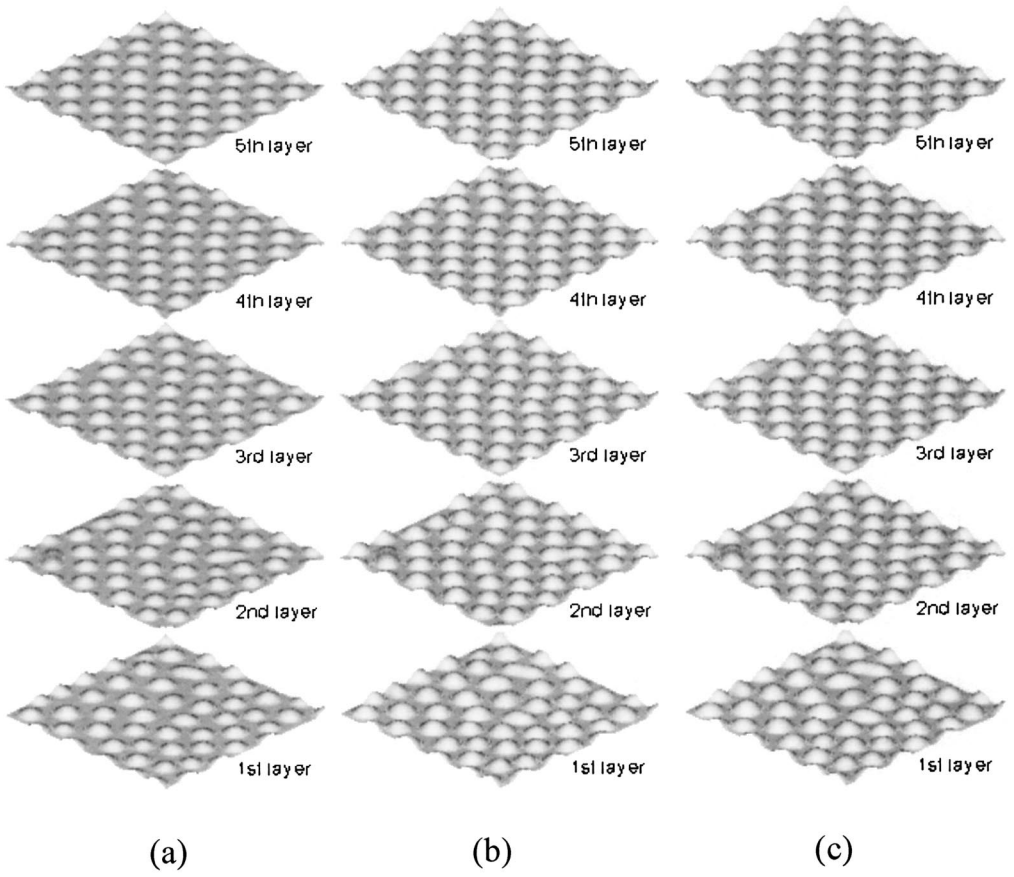

FIG. 1. The surface morphologies at the end of each dot layer growth. With the proper choice of system parameters, strong ordered dot arrays are obtained after a number of superlattice growth periods. (a) $\eta_* = 0.005\lambda_0/t_0$ and $\mu_{0*} = 5\Omega\omega_0$; (b) $\eta_* = 0.008\lambda_0/t_0$ and $\mu_{0*} = 5\Omega\omega_0$; and (c) $\eta_* = 0.005\lambda_0/t_0$ and $\mu_{0*} = 8\Omega\omega_0$. The same initial surface, spacer layer and interruption time are used. (The lateral size is 32. Along the growth direction, the scale has been magnified by 2.)

vertical correlation is preferred, while when the spacer layer is thick, a vertical anticorrelation is preferred. The current predictions show that the anticorrelation is more effective to achieve a strong ordering of quantum dots in superlattices.

II. FORMULATIONS

The island formation and arrangement of superlattices can be affected by many factors, such as, mismatch strain, spacer layer thickness, surface mobility, interface diffusion, deposition rate and time, segregation, spacer layer surface roughness, and buried island distribution. It has been shown that the effect of segregation on the film surface and spacer layer surface roughness appear insignificant,[5,26] therefore are not considered here. In addition, it is believed that the interface diffusion is significantly slower than the surface diffusion, and hence is omitted. In this paper, the effects of strain mismatch, deposition rate and time, spacer layer thickness, and buried island distribution on the self-organized growth of quantum dot superlattices will be examined.

In the current computer modeling, a three-dimensional kinetic model is developed to simulate quantitatively the dot formation and ordering in superlattices under growth. It is capable of modeling heteoepitaxial thin film systems with

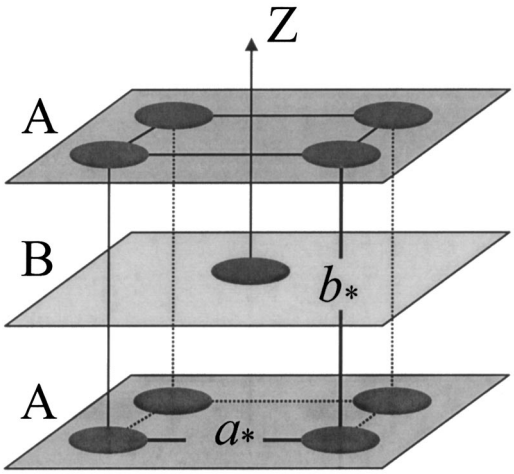

FIG. 2. The unit cell for the bct superlattice. The quantum dot array adopts an alternative *ABAB* stacking sequence. The lattice spacing along the growth direction is $b_* = 5.2$. The dots in the growth plane adopt a squared lattice with spacing $a_* = 4.5$.

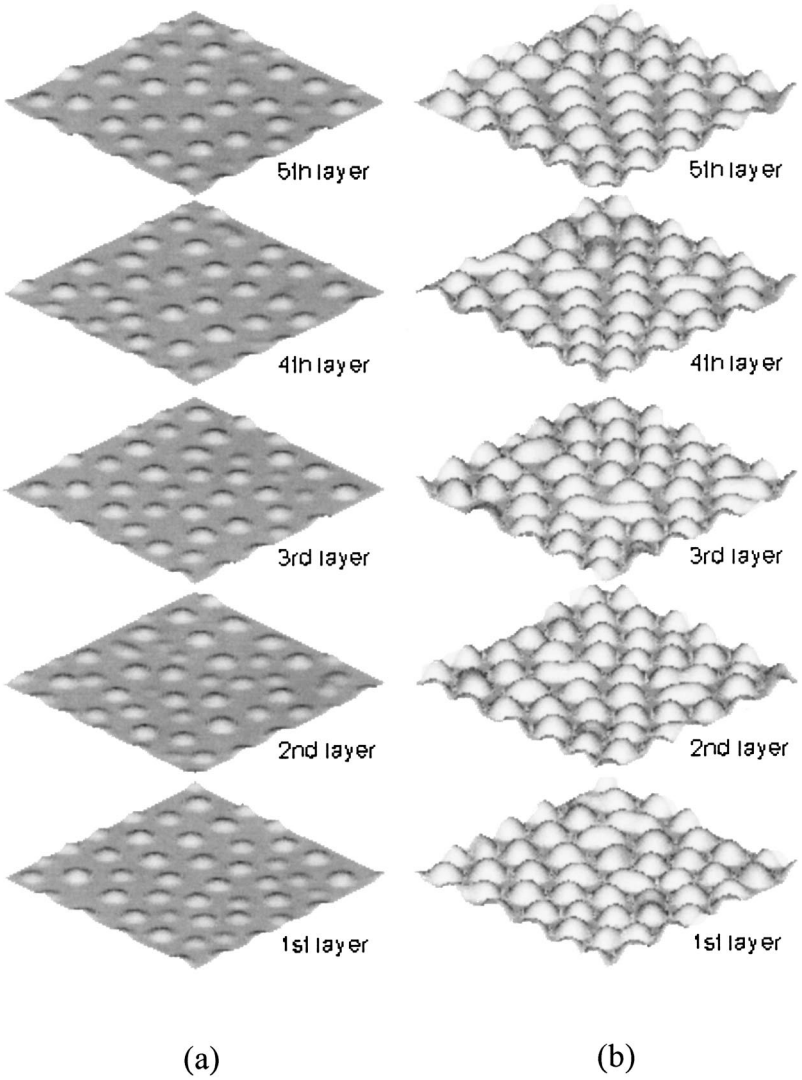

FIG. 3. The surface morphologies at the end of each dot layer growth. The growth rate also affects the ordering of dots in superlattices. (a) At a low growth rate, $\eta_* = 0.002\lambda_0/t_0$ and $\mu_{0*} = 5\Omega\omega_0$, dot ripening occurs and the density of dots gradually decreases, (b) At a high growth rate, $\eta_* = 0.015\lambda_0/t_0$ and $\mu_{0*} = 5\Omega\omega_0$, the formation of dots is not complete. (The lateral size is 32. Along the growth direction, the scale has been magnified by 2.)

the Stranski-Krastanov (SK) growth mode.[9,10] To model the SK growth mode, the wetting layer on top of the substrate is modeled as a transition layer with a linearly varied mismatch strain along the growth direction.[19,20,28] The transition layer can be assumed to be an intermixing phase of the substrate and the film.[28,29] It is assumed that the transition layer is very thin so that it will not affect the morphologic evolution of the film surface. The substrate, dot, and spacer layers are elastically isotropic solids with the same elastic properties representative of semiconductors. The substrate and spacer layers are of the same lattice spacing, which is different from that of the dot layers.

During epitaxial growth, the surface morphology will evolve. Therefore, tuning the growth rate and growth time gives one an additional degree of freedom to control the self-organization of the epitaxial growth. After the formation of the first layer of quantum dots, subsequently a spacer layer is grown on the dot layer surface. Here it is assumed that the interface diffusion along the film and the space layer is negligibly small[24,25] and the termination of the spacer layer surface is flat;[11,12] the shape and properties of the spacer layer are known and there is no need to model the growth of spacer layers. Subsequently, another transition layer and film layer are grown on the spacer layer surface. Again during the growth, the film will roughen and form dots. This process is repeated and a multilayer quantum dot superlattice can be obtained through computer simulations.

The growth of quantum dot superlattices is modeled using a thick large substrate bonded to a rigid foundation, and a thin transition layer is grown on the substrate to consider the wetting effect. The simulation temperature is above the roughening transition temperature, hence, no faceted surface exists on the film surface. The surface of the transition layer is perturbed randomly to model the surface roughness. It should be noted that without stress in the layer, the perturbed surface simply decays and evolves into a flat surface. This means that the collective fluctuation of the surface (capillary waves)[30,31] is not included in the present continuum treatment. The film which is strained elastically is grown on the transition layer. the film is unstable and will spontaneously roughen and form dots because of surface diffusion.[21–25] Here the film is treated as a linear-elastic solid and the displacement due to mechanical loading is small. Therefore, changes in shape caused by the elastic deformation do not

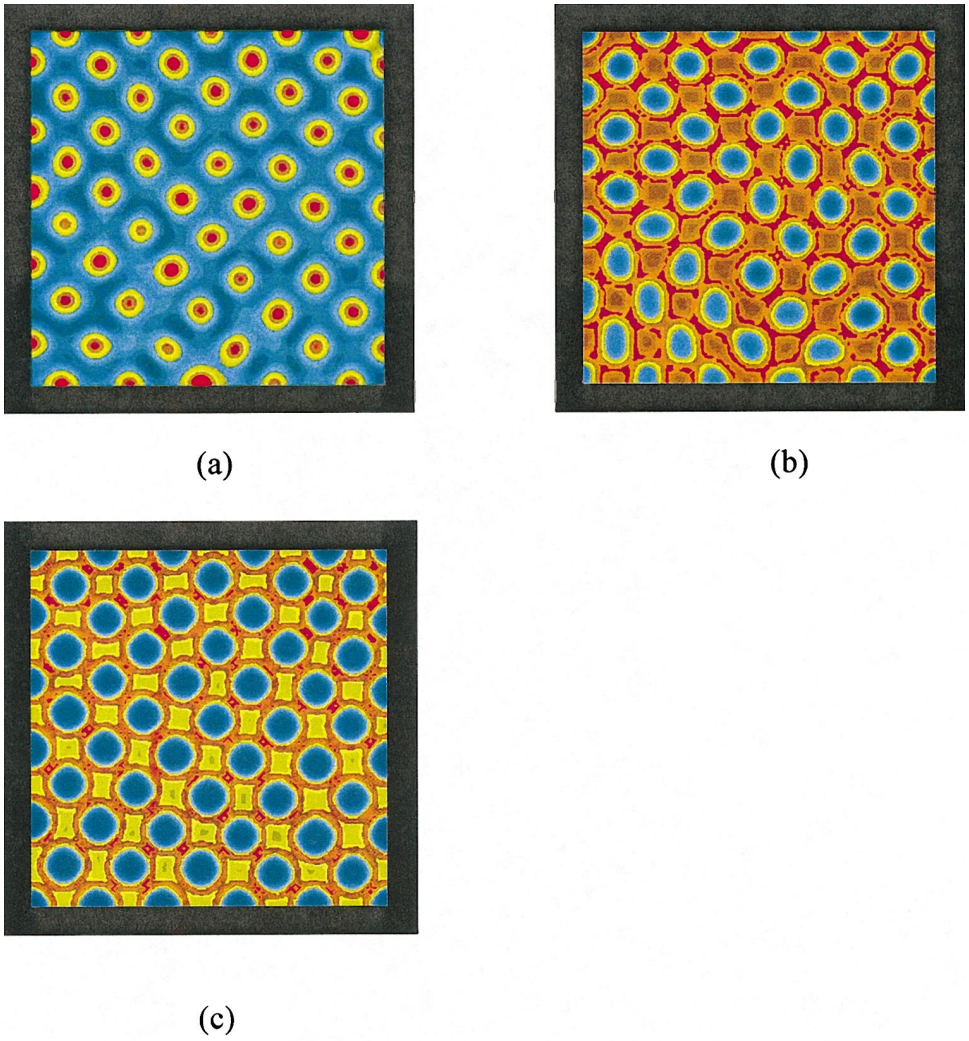

FIG. 4. (Color) The contour plots of the chemical potential at different times during the fifth film layer growth for the case of $\eta_* = 0.007\lambda_0/t_0$ and $\mu_{0*} = 5\Omega\omega_0$. (a) Before the fifth film layer growth, the chemical potential maxima on the spacer layer surface (red spots) are very regular, but the minima are not. (b) A regular array of chemical potential minima (blue spots), which correspond to islands, form after the deposition of the fifth layer starts. It can be seen that each maximum on the spacer layer surface corresponds exactly to an anticorrelated position, however, there is no such one-to-one relationship between a minimum and a dot. (c) At the end of the fifth layer growth, the chemical potential minima (blue spots) evolve into a perfectly regular array, which corresponds to a perfectly regular island array. (The lateral size is 32.)

influence diffusion on the surface.

Surface diffusion is driven by a variation in chemical potential which causes atoms to migrate from regions of high chemical potential to those of low chemical potential. There are two contributions to the chemical potential of an atom on the surface of the thin film.[21] The first is the energy of the surface itself, while the second is due to the elastic energy stored in the volume of material associated with a surface atom. Thus, the chemical potential μ is[21]

$$\mu = \Omega(\omega - \kappa\gamma), \tag{1}$$

where ω is the strain energy density on the film surface, γ is the surface energy, κ is the sum of two principal curvatures, and Ω is the atomic volume. The strain energy is given by $\omega = C_{ijkl}\varepsilon_{ij}\varepsilon_{kl}/2$, where C_{ijkl} are the elastic constants and the strain field ε_{ij} is a function of the displacement field $u_i(x_j)$, that is, $\varepsilon_{ij} = (u_{i,j} + u_{j,i})/2$. It should be mentioned that κ is positive if the center of curvature is in the direction of the outward pointing normal. The chemical potential of the bulk is assumed to be zero.

For temperatures above the roughening transition temperature one expects the Wilson-Frenkel growth mode, i.e., a linear law to hold between the growth rate and the chemical potential differences between the vapor phase and the surface.[31] If the growth rate is ν_g and the vapor phase chemical potential is μ_0, then,

$$\nu_g = \eta(\mu_0 - \mu), \tag{2}$$

where η is a growth parameter which depends on the sticking coefficient, temperature, and the mass of the vapor atom.

The normal velocity on the surface in the reference configuration at which material is deposited or evaporated from an element on the surface is related to surface diffusion and deposition, that is,

$$\nu_n = D\nabla_s^2\mu + \eta(\mu_0 - \mu), \tag{3}$$

where D is the material system parameter which is related to mass surface diffusion coefficient and temperature and ∇_s^2 is the surface Laplacian operator. By assuming a symmetrical condition and applying the surface divergence theorem (3) may be rewritten in a weak form as

$$\int_S \nu_n \delta\nu_n dA = \int_S D\mu\nabla_s^2(\delta\nu_n) + \eta(\mu_0 - \mu)\delta\nu_n dA. \quad (4)$$

This equation may be solved for ν_n using the finite element method.[19] However, since Eq. (4) is stiff due to the mean curvature term κ in the chemical potential μ, a finite element method with a semi-implicit Euler scheme is introduced to solve this equation. The reference surface configuration is perturbed by a small displacement u_n along the normal direction of the surface within a small time interval Δt; $u_n = \nu_n \Delta t$ is chosen for the forward Euler numerical scheme. The new surface curvature after the small perturbation is

$$\kappa' = \kappa + \nabla_s^2 u_n + u_n(\kappa^2 - 2K), \quad (5)$$

where K is the Gaussian curvature. Replacing κ in Eq. (4) with κ' and rearranging the equation, the semi-implicit scheme may be written as

$$\int_S u_n \delta\nu_n + \Delta t\Omega\gamma[\nabla_s^2 u_n + u_n(\kappa^2 - 2K)](D\nabla_s^2 \delta\nu_n - \eta\delta\nu_n)dA = \Delta t\Omega \int_S (\omega - \kappa\gamma)(D\nabla_s^2 \delta\nu_n - \eta\delta\nu_n) + \eta\mu_0 \delta\nu_n dA \quad (6)$$

and solved for u_n using the finite element method. The equations governing surface diffusion of the film are completed by the constraints at the surface boundaries. A symmetrical condition is used to prescribe the behavior of the boundaries and requires the mass flux and the tangential component of the surface along the normal of the boundary to vanish.

The procedure of simulating the quantum dot superlattice growth is as follows. The growth starts on the random surface of the transition layer bonded on the substrate. To determine the surface evolution, Eq. (6) is to be computed. Suppose the shape of the film surface configuration at time t is known. The deformation and diffusion that occur during a subsequent infinitesimal time interval Δt is to be determined. First, the displacement field u_i, strain field ε_{ij}, and strain energy density distribution need to be computed. To do so, the equations of mechanical equilibrium using the configuration at t as reference are solved. Secondly, based on the surface configuration, the surface curvatures can be calculated. Next, the surface diffusion equation (6) is solved to determine the velocity of the surface in the reference configuration at time t. The shape of the surface during the time interval Δt is then deduced. These steps are repeated to compute the shape of the surface during the dot layer growth. Once the first dot layer growth is finished, a spacer is added on the dot layer. The spacer layer surface is assumed to be flat since the spacer surface roughness is neglected. On top of the flat spacer layer, another transition layer is added. Then the second dot layer growth on the transition layer is commenced. The calculation steps for the island formation and evolution of the second dot layer are the same as the first dot layer. The procedure is repeated to compute the growth process of the quantum dot superlattice. It is noted that the stress analysis in the subsequent growth should include the substrate and all spacer, transition, and dot layers. Since the surface configuration after each time interval Δt has been changed, finite element remeshing is required. In addition, with the addition of the spacer layer and transition layer, finite element remeshing is also required.

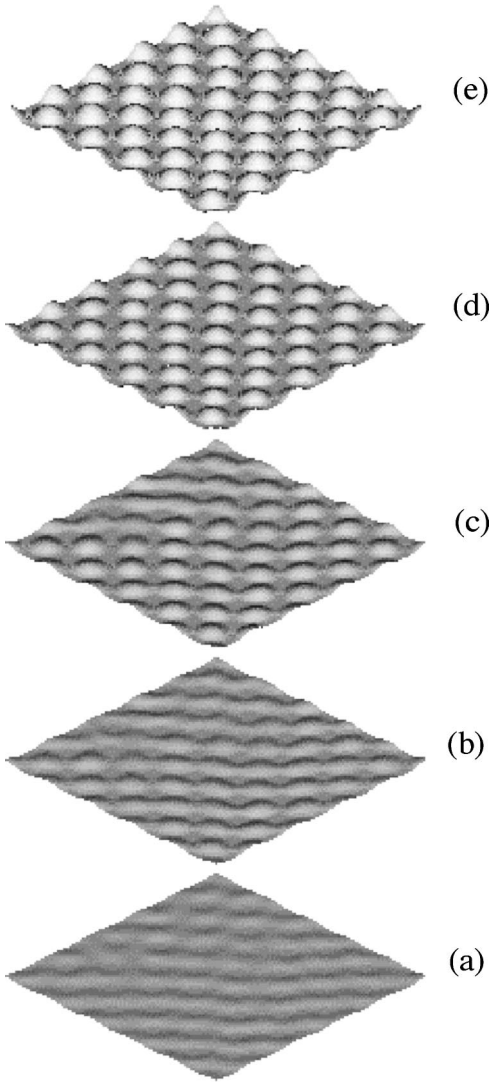

FIG. 5. Surface morphologies at the end of the fifth dot layer growth with $\eta_* = 0.005\lambda_0/t_0$ and $\mu_{0*} = 8\Omega\omega_0$. (a) Pits are formed first on the surface. (b) The pits grow and expel the surrounding mass. (c) The pileup mass forms islands. (d) A uniform and regular array of islands are formed. (e) The dots still remain uniform and regular but grow with an increase in growth time. (The lateral size is 32. Along the growth direction, the scale has been magnified by 2.)

In this work, massive parametric studies to investigate quantum dot morphologic evolution and self-organization during the growth process have been conducted. To present the results, a dimensionless length scale and time scale is used as follows: $\lambda_* = \lambda/\lambda_0$, $t_* = t/t_0$, where $\lambda_0 = \gamma/\omega_0$ and $t_0 = \gamma^3/(\omega_0^4 D\Omega^2)$, where ω_0 is the strain energy density in a perfectly flat film.

III. RESULTS AND DISCUSSION

In the massive parametric studies, the effects of the simulation size, the initial surface roughness, the spacer layer thickness, the growth time, the growth parameter η, and the vapor chemical potential μ_0 are investigated. Our parametric studies show that all the conclusions still apply as long as the cell lateral dimension is larger than 16, the substrate thickness is larger than 5, and the transition layer thickness is less than 0.1. For all the simulation results reported here, the dimensionless length and width of our simulation cells are the same, i.e., 32, the dimensionless substrate thickness is 8.0, the dimensionless transition layer thickness 0.1.

The simulations have reproduced many interesting experimental observations, such as dot alignment, dot misalignment, and dot discontinuity.[11–18] Of particular interest is the prediction that with a proper choice of system parameters, a perfectly uniform and regular bct quantum dot superlattice can be obtained. We found that when the dimensionless spacer layer thickness is chosen to be 2.5 and the dimensionless interruption time is 5, the dimensionless growth parameter η_* is between $0.004\lambda_0/t_0$ and $0.01\lambda_0/t_0$ and the dimensionless vapor chemical potential μ_{0*} is between $4\Omega\omega_0$ and $9\Omega\omega_0$, a strong ordering of quantum dots occurs and a perfectly ordered quantum dot superlattice is obtained. Examples are shown in Fig. 1(a) with $\eta_*=0.005\lambda_0/t_0$ and $\mu_{0*}=5\Omega\omega_0$, in Fig. 1(b) with $\eta_*=0.008\lambda_0/t_0$ and $\mu_{0*}=5\Omega\omega_0$, and in Fig. 1(c) with $\eta_*=0.005\lambda_0/t_0$ and $\mu_{0*}=8\Omega\omega_0$. There are several features which characterize the strong ordering of the quantum dot self-organization in the growth window. First, after a few layers of superlattice growth periods, the top dot arrays become increasingly uniform and regular. These ordered dots adopt a squared array. The separation of the dots appears to be insensitive to the variation of the initial random surfaces, the kinetic parameter η and the vapor phase chemical potential μ_0. Secondly, the dots in the two dot arrays separated by a spacer layer are anticorrelated, i.e., the stacking sequence is of the *ABAB* form as shown in Fig. 2. The spacer layer thickness is responsible for this transition, which was also observed in the annealing cases.[20] Thirdly, with the increase of deposition rate, i.e., with the increase of the kinetic parameter η and the vapor phase chemical potential μ_0, the spacing and the pattern of the dot arrays remain the same. However, the dot size is increased with the increase of the deposition rate which can be seen from Figs. 1(b) and 1(c). Finally, within this window, as long as the initial film surfaces remain roughly random, i.e., without strong preferential perturbation directions, the strong ordering of the quantum dot self-organization is insensitive to the initial surface conditions.

It is showed that after a few periods of superlattice growth, the arrangement of quantum dots in the superlattices adopts a bct lattice with a squared array in the growth plane and an alternative *ABAB* stacking sequence along the growth direction. The unit cell for the bct superlattice is shown in Fig. 2. The lattice spacing of the dot array in the growth plane is $a_*=4.5$. The lattice spacing along the growth direction is $b_*=5.2$. The basis vectors of the superlattice in the real space are

$$\begin{Bmatrix} \mathbf{a}_1 \\ \mathbf{a}_2 \\ \mathbf{a}_3 \end{Bmatrix} = \begin{bmatrix} a_*/\sqrt{2a_*^2+b_*^2} & a_*/\sqrt{2a_*^2+b_*^2} & -b_*/\sqrt{2a_*^2+b_*^2} \\ a_*/\sqrt{2a_*^2+b_*^2} & a_*/\sqrt{2a_*^2+b_*^2} & b_*/\sqrt{2a_*^2+b_*^2} \\ a_*/\sqrt{2a_*^2+b_*^2} & -a_*/\sqrt{2a_*^2+b_*^2} & b_*/\sqrt{2a_*^2+b_*^2} \end{bmatrix} = \begin{bmatrix} 0.548 & 0.548 & -0.633 \\ 0.548 & 0.548 & 0.633 \\ 0.548 & -0.548 & 0.633 \end{bmatrix}. \tag{7}$$

For a perfect body-centered cubic lattice, $a_*/b_*=1$, however, for the current situations, the ratio is 0.87. The current quantum dot superlattice can be thought of as a perfect body-centered cubic lattice that is expanded by 13% along the growth direction.

In the growth window, the current ordered bct quantum dot superlattices can be tuned in two ways. First, the island spacing can be tuned by the change of the lattice mismatch between the film layers and the substrate since the characteristic wavelength in the system is inversely proportional to the square of mismatch strain. Therefore, with the increase of lattice mismatch between the spacer layers and the dot layers, the dot size and spacing will be decreased and vice versa. Secondly, the size of the dots can be tuned by the change of the growth rate. For an increase in the growth rate, the dot size will increase while the dot spacing of the bct superlattice remains the same.

The previous theoretical analyses predicted that for elastically isotropic materials, the strain energy minima on the growth surface occur right above the buried dots, and therefore the dots in the multilayer should be aligned vertically,[12,13] while for elastically anisotropic materials, the strain energy minima no longer occur right above the buried dots, therefore misalignment of the dots occurs.[5,14,15] It is believed that the strain energy density minima on top of the spacer layer surface provide the preferential sites for dot formation, and the ordering of the dot self-organization is due to the ordering of the strain energy density minima during the film growth.[5,12–15,20]

The results show that the current strong ordering of the dot self-organization is due to different reasons. First, the anticorrelation in the present case is not due to the elastic anisotropy,[5,14] but due to the effect of the spacer layer thickness. Secondly, the strong ordering is also closely related with growth time and growth rate. At a lower growth rate, the surface diffusion rate may be relatively higher than the growth rate. As a consequence, island ripening occurs and the dot number density gradually decreases during the super-

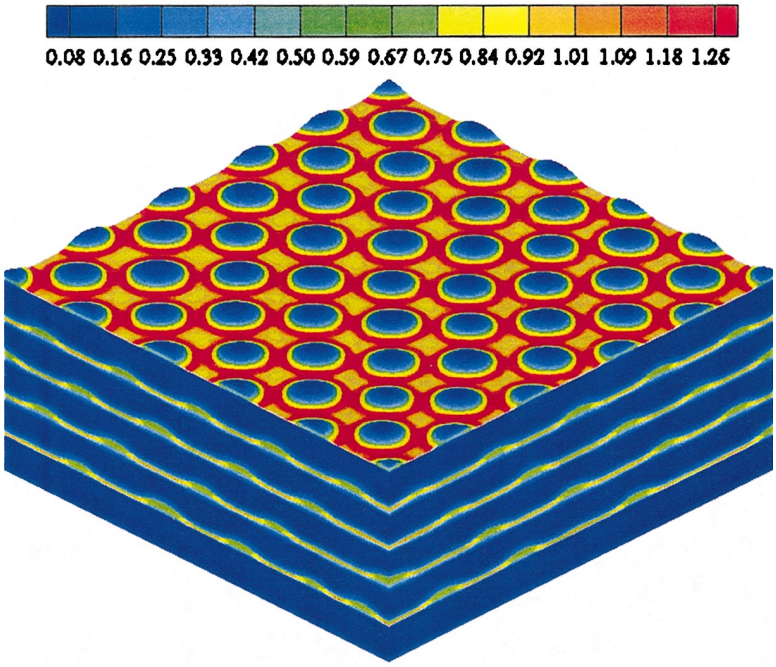

FIG. 6. (Color) Normalized strain energy distribution on the surface at the end of the fifth dot layer growth. The strain energy distribution becomes very regular on the fifth island layer surface due to the interactions of the buried islands and surface islands. The strain energy minima are located on the island tops while the high strain energy density is around the island bottom edge. (The lateral size is 32. Only part of the substrate is shown.)

lattice growth as shown in Fig. 3(a). While at a higher growth rate, the surface diffusion rate may be relatively lower than the growth rate. As a consequence, the formation of islands is incomplete as shown in Fig. 3(b). Thirdly, the strong ordering of the dot self-organization in the present cases is not due to the ordering of the strain energy density minima atop of the spacer layer surface,[5,12–15,20] but due to the ordering of the strain energy density maxima on the spacer layer surface and the interaction between the surface islands and the buried islands. Figure 4(a) shows the contour plot of the chemical potential distribution on the spacer layer surface before the fifth superlattice layer growth. (If the spacer layer surface is flat, the chemical potential is equal to $\Omega\omega$.) It can be clearly seen that the strain energy maxima are very regular, but the minima are not. Figure 4(b) shows the contour plot of the chemical potential distribution at the early stage of the fifth film layer growth. It can be seen that both the chemical potential minima and the chemical potential maxima form a regular array. Figure 4(c) shows the contour plot of the chemical potential distribution at the end of the fifth film layer growth. The chemical potential minima develop a perfectly regular anticorrelated array, which corresponds to a perfectly regular island array. Apparently, it can be seen that each maximum on the spacer layer surface shown in Fig. 4(a) exactly corresponds to a correlated position without an island as shown in Fig. 4(c). However, there is no such one-to-one relationship between the minima in Fig. 4(a) and the minima (the island positions) in Fig. 4(c). Therefore, the previous understanding cannot explain the surprising result in the present case since before the fifth film layer growth, the strain energy maxima are regular, but the minima are not. Hence, the ordering of the dot self-organization in the early stage is attributed to the ordering of the strain energy density maxima on top of the spacer layer surface, rather than the strain energy density minima on top of the spacer layer surface. Detailed study revealed the underlying reason: From Fig. 4(a), it can be seen that the strain energy density minima are not only disordered, but are also shallow. Hence, they are unlikely to trap dots. However, the strain energy density maxima are not only ordered, but also of a high magnitude. During the superlattice growth, the film material will diffuse away from the positions where their strain energy densities are maximum. In addition, due to the high surface chemical potentials at these positions, the deposition rate is low and, as a result, pits develop. Therefore, the ordered pits, rather than the ordered dots, first appear on the growth surfaces as shown in Fig. 5(a). To reduce strain energy, the mass that is repulsed away from its neighboring pits tends to increase its aspect ratio to form an island as shown in Figs. 5(b), 5(c). Since the strain energy density at the neighboring pits is high, the formed island tries to keep away from the neighboring pits so as to reduce its energy. Therefore the most favorable place will be at the center among its neighboring pits as shown in Figs. 5(b), 5(c), that is, the anticorrelated position [a blue spot in Fig. 4(b)]. A 3D strain energy contour at the end of the fifth dot layer growth is given in Fig. 6. The strain energy minima are located on the island tops while the high strain energy density is around the island edges. The high strain energy gives rise to high surface chemical potential, causing the mass on the wetting layer to diffuse to the island tops. Consequently, an ordered dot array is developed as shown in Figs. 4(c) and 5(d), 5(e).

It has been shown that the interactions between the surface islands and the buried islands also contribute to island ordering.[5,26,27] This is also true in the present studies since the results show that no reorganization occurs once the ordered island array is formed at an early stage. Hence, in the growth window the interactions between the surface islands and the buried islands not only favor the ordering at the early stage of island formation, but also maintain the ordering at the subsequent growth stage.

IV. CONCLUSIONS

The computer simulations performed in this study have identified a growth window in which the growth of high-density, high-ordered quantum dot superlattices can be controlled. The perfectly ordered self-organized quantum dots are arranged in a body-centered tetragonal superlattice. The dot spacing is insensitive to growth rate, however, the size of the dots can be tuned through the change of growth rate. A physical phenomenon for the ordering of the self-organized quantum dot superlattices was discovered. The ordering is controlled by the ordering of the strain energy density maxima, rather than by the ordering of the strain energy density minima. This provides a promising guideline for the fabrication of novel quantum dot-based devices.

ACKNOWLEDGMENT

The authors thank A. F. Bower for helpful discussions.

*Corresponding author. Email address: maszyw@nus.edu.sg

[1] A. P. Alivistas, Science **271**, 933 (1996).
[2] R. Leon, P. M. Petroff, D. Leonard, and S. Fafard, Science **267**, 1966 (1995).
[3] D. Bimberg, M. Grundmann, and N. N. Ledentsov, *Quantum Dot Heterostructures* (Wiley, Chichester, 1998).
[4] C. B. Murray, C. R. Kagan, and M. G. Bawendi, Science **270**, 1335 (1995).
[5] G. Springholz, V. Holy, M. Pinczolits, and G. Bauer, Science **282**, 734 (1998).
[6] J. A. Floro, G. A. Lucadamo, E. Chason, L. B. Freund, M. Sinclair, R. D. Twesten, and R. Q. Hwang, Phys. Rev. Lett. **80**, 4717 (1998).
[7] G. Medeiros-Ribeiro, A. M. Bratkovski, T. I. Kimins, D. A. A. Ohlberg, and R. S. Williams, Science **279**, 353 (1998).
[8] R. M. Tromp, F. M. Ross, and M. C. Reuter, Phys. Rev. Lett. **84**, 4641 (2000).
[9] P. Sutter and M. G. Lagally, Phys. Rev. Lett. **84**, 4637 (2000).
[10] D. Pan, Y. P. Zeng, J. M. Li, C. H. Zhang, M. Y. Kong, H. M. Wang, C. Y. Wang, and J. Wu, J. Cryst. Growth **175/176**, 760 (1997).
[11] Y. Nakata, Y. Sugiyama, T. Futatsugi, and N. Yokoyama, J. Cryst. Growth **175/176**, 713 (1997).
[12] J. Tersoff, C. Teichert, and M. G. Lagally, Phys. Rev. Lett. **76**, 1675 (1996).
[13] Q. Xie, A. Madhukar, P. Chen, and N. P. Kobayashi, Phys. Rev. Lett. **75**, 2542 (1995).
[14] V. A. Shchukin, N. N. Ledentsov, and D. Bimberg, Physica E **9**, 140 (2001).
[15] V. Holy, G. Springholz, M. Pinczolits, and G. Bauer, Phys. Rev. Lett. **83**, 356 (1999).
[16] O. Kienzle, F. Ernst, M. Ruhle, O. G. Schmidt, and K. Eberl, Appl. Phys. Lett. **74**, 269 (1999).
[17] M. Strassburg, V. Kutzer, U. W. Pohl, A. Hoffman, I. Broser, N. N. Ledentsov, D. Bimberg, A. Rosenauer, U. Fischer, D. Gerthsen, I. L. Krestnikov, M. V. Maximov, P. S. Kop'ev, and Zh. I. Alferov, Appl. Phys. Lett. **72**, 942 (1998).
[18] H. Li, J. Wu, Z. Wang, and T. Daniels-Race, Appl. Phys. Lett. **75**, 1173 (1999).
[19] Y. W. Zhang, Appl. Phys. Lett. **74**, 1809 (1999).
[20] P. Liu, Y. W. Zhang, and C. Lu, Appl. Phys. Lett. **80**, 3910 (2002).
[21] R. J. Asaro and W. A. Tiller, Metall. Trans. **3**, 1789 (1972).
[22] D. J. Srolovitz, Acta Metall. **37**, 621 (1989).
[23] H. Gao, J. Mech. Phys. Solids **42**, 741 (1994).
[24] B. J. Spencer, P. W. Voorhees, and J. Tersoff, Phys. Rev. Lett. **84**, 2449 (2000).
[25] B. J. Spencer, P. W. Voorhees, and J. Tersoff, Phys. Rev. B **64**, 235318 (2001).
[26] C. Priester, Phys. Rev. B **63**, 153303 (2001).
[27] L. E. Shilkrot, D. J. Srolovitz, and J. Tersoff, Appl. Phys. Lett. **77**, 304 (2000).
[28] R. V. Kukta and L. B. Freund, J. Mech. Phys. Solids **45**, 1835 (1997).
[29] K. Jacobi, Prog. Surf. Sci. **71**, 185 (2003).
[30] S. Krukowski and F. Rosenberger, Phys. Rev. B **49**, 12464 (1994).
[31] H. Muller-Krumbhaar, in *1976 Crystal Growth and Materials*, edited by E. Kaldis and H. J. Scheel (North-Holland, Amsterdam, 1997).